Natural and anthropogenic processes contributing to metal enrichment in surface soils of central Pennsylvania

A. M. L. Kraepiel \cdot A. L. Dere \cdot E. M. Herndon \cdot S. L. Brantley

Received: 31 July 2014/Accepted: 3 January 2015 © Springer International Publishing Switzerland 2015

Abstract Metals in soils may positively or negatively affect plants as well as soil micro-organisms and mesofauna, depending on their abundance and bioavailability. Atmospheric deposition and biological uplift commonly result in metal enrichment in surface soils, but the relative importance of these processes is not always resolved. Here, we used an integrated approach to study the cycling of phosphorus and a suite of metals from the soil to the canopy (and back) in a temperate watershed. The behavior of elements in these surface soils fell into three categories.

Responsible Editor: Melany Fisk.

Electronic supplementary material The online version of this article (doi:10.1007/s10533-015-0068-5) contains supplementary material, which is available to authorized users.

A. M. L. Kraepiel (⊠)
Department of Chemistry, Princeton University,
Princeton, NJ 08544, USA
e-mail: kraepiel@princeton.edu

A. L. Dere · E. M. Herndon · S. L. Brantley
Department of Geosciences and Earth and Environmental
Systems Institute, Pennsylvania State University,
University Park, PA 16802, USA

A. L. Dere

Department of Geography/Geology, University of Nebraska at Omaha, Omaha, NE 68182, USA

Published online: 15 January 2015

E. M. Herndon Department of Geology, Kent State University, Kent, OH 44242, USA First, Al, Fe, V, Co, and Cr showed little to no enrichment in the top soil layers, and their concentrations were determined primarily by soil production fluxes with little influence of either atmospheric inputs or biological activity. Second, P, Cu, Zn and Cd were moderately enriched in surface soils due to a combination of atmospheric deposition and biological uplift. Among the metals we studied. Cu, Zn and Cd concentrations in surface soils were the most sensitive to changes in atmospheric deposition fluxes. Finally, Mo and Mn showed strong enrichment in the top soil layer that could not be explained strictly by either current atmospheric deposition or biological recycling processes, but may reflect both their unique chemistry and remnants of past anthropogenic fluxes. Mn has a long residence time in the soil partly due to intense biological uplift that retains Mn in the top soil layer. Mo, in spite of the high solubility of molybdate, remains in the soil because of strong binding to natural organic matter. This study demonstrates the need to consider simultaneously the vegetation and the soils to understand elemental distribution within soil profiles as well as cycling within watersheds.

Keywords Metal · Soils · Biological uplift · Atmospheric deposition · Pollution

Introduction

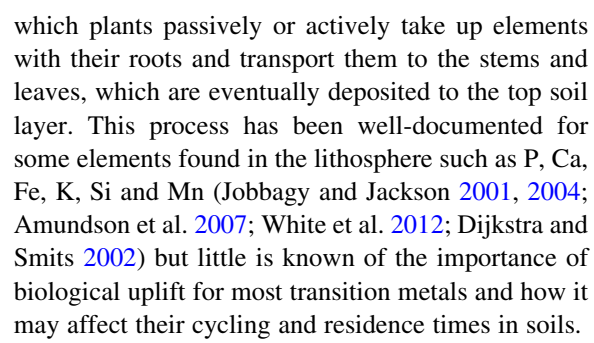
The cycling of transition metals in soils is of particular interest because many of these metals are either toxic



to biota or required for essential biological reactions depending on their concentrations and bioavailability. Metal contamination in soils is often a concern, either because it negatively affects plant growth or because it results in high (toxic) metal concentrations in crops and/or animal feed (e.g., Kinkle et al. 1987; Roy and McDonald 2013). The opposite situation may also be encountered, where the bioavailability of some metals is insufficient to sustain key biological reactions. For example, a number of studies have shown that Mo can be a limiting nutrient for nitrogen fixation in temperate and tropical soils, potentially affecting the overall input of new nitrogen and soil fertility (Silvester 1989; Gupta 1997; Barron et al. 2009; Jean et al. 2012; Wurzburger et al. 2012; Darnajoux et al. 2014; Hodkinson et al. 2014).

The vertical distributions of metals and other elements with soil depth are the result of multiple interconnected processes, such as physical and chemical weathering, atmospheric deposition, leaching and biological activity. The interaction of these processes sometimes results in complex concentration patterns with depth, but simple depletion or enrichment profiles are also common. Although surface depletion is sometimes observed due to weathering or dilution with metal-poor plant biomass, many transition metals show high concentrations in the top soil layer compared to deeper depths (Teutsch et al. 1999, Hernandez et al. 2003; Tyler 2004; Kobler et al. 2010; Herndon et al. 2011; Sucharova et al. 2012). Depending on the metal and the geographical location of the study, surface enrichment has been interpreted as a result of atmospheric deposition (addition profile) or of biological uplift (biogenic profile) (Reimann et al. 2009; Herndon et al. 2011; Brantley and White 2009; Brantley and Lebedeva 2011; Sucharova et al. 2012). Atmospheric deposition results in a net addition of metals to the soil, whereas biological uplift creates a vertical redistribution of metals that become progressively depleted in the deep soil and enriched in the top soil layer that contains dead plant biomass.

Atmospheric deposition fluxes are often significantly affected (and sometimes dominated) by anthropogenic emissions, which originate from various sources including mining, smelting and refining of metals, burning of fossil fuels, and production and use of metallic commercial products (Nriagu 1990). Here, we define biological uplift as the process through



In addition to being responsible for biological uplift, plants also produce large quantities of natural organic matter (NOM) that accumulate in the soil and at the soil surface. Strong binding of metals to NOM reduces leaching rates and retains metals in the upper soil layers and may contribute to surface enrichment for metals added by atmospheric deposition and/or by biological uplift. Unraveling the role played by biology in shaping metal concentration gradients with soil depth thus requires an integrated approach accounting for both the soil and the vegetation.

We conducted a study of metal cycling in the Susquehanna Shale Hills Critical Zone Observatory (SSHO) in Pennsylvania, USA. Specifically, we investigated the vertical distribution of elements from canopy (green) leaves to litterfall and along the soil profile from the O horizon to the parent rock at several ridgetop sites dominated by different tree species. We examined phosphorus (P) and a suite of metals (Al, Fe, Mn, V, Cr, Co, Cu, Zn, Mo, Cd) with contrasting sources, biological cycles, history of atmospheric pollution and affinity for NOM to identify the roles of atmospheric inputs and biology in the distribution of metals in soils at the SSHO.

Materials and methods

Study site

The SSHO is a small 8 ha catchment with an intermittent stream underlain by organic-poor, iron-rich shale of the Silurian Rose Hill Formation. Mean annual temperature is 10 °C and mean annual precipitation is 107 cm (Jin et al. 2010). Ridgetop and planar slope soils are well-drained, shallow Dystrudepts while swale and valley floor soils are more poorly drained, deeper Hapludults (Lin 2006). The dominant tree



species include oak, hickory, maple, hemlock and pine (Lin 2006). The geology, ecology and hydrology of the SSHO have been extensively characterized (Jin et al. 2010; Kuntz et al. 2011; Lin 2006; Lin et al. 2006; Ma et al. 2010; Naithani et al. 2013; West et al. 2013). Currently the SSHO is located in a relatively pristine forest in a low population density region; however, the site was once located near one of the centers of the iron industry in the 1800s (Herndon et al. 2011) and was subject to periodic deforestation until the early 1900s (Jin et al. 2010). Recent papers demonstrate Mn and Pb enrichments from coal-burning and iron smelting inputs at the SSHO and provide a conceptual and experimental framework for our study (Herndon and Brantley 2011; Herndon et al. 2011; Ma et al. 2015).

Sampling

Soil cores

Soil cores (n = 9) were collected using a 2-inch diameter hand auger at three ridgetop sites located along the south and north slopes of the catchment (G1,

G2 and G3, Fig. 1) in September 2009. All soils are well-drained but are distinguished by different relative soil moisture regimes, with average soil moisture increasing from site G3 < G1 < G2 (Lin et al. 2006). At each site, soil samples were collected on the ridgetop where at least one pine, hickory or oak tree with a diameter >20 cm at breast height (1.3 m above the ground surface) was in close proximity. Beginning at the surface of the mineral soil and excluding the organic horizon, soils were collected in 5 cm depth increments until 20 cm, then in 10 cm increments until reaching the bedrock interface, defined as the point of manual refusal by hand augering. The surface of the mineral soil is defined as depth d = 0 cm and depths recorded below the surface are reported as negative numbers. The A horizon (top soil layer) is defined as the upper 0-5 cm of the soil (-5 cm < d < 0).

Green leaves

Green leaves were collected from oak (Q. alba and Q. prinus), hickory (C. tormentosa and C. glabra),

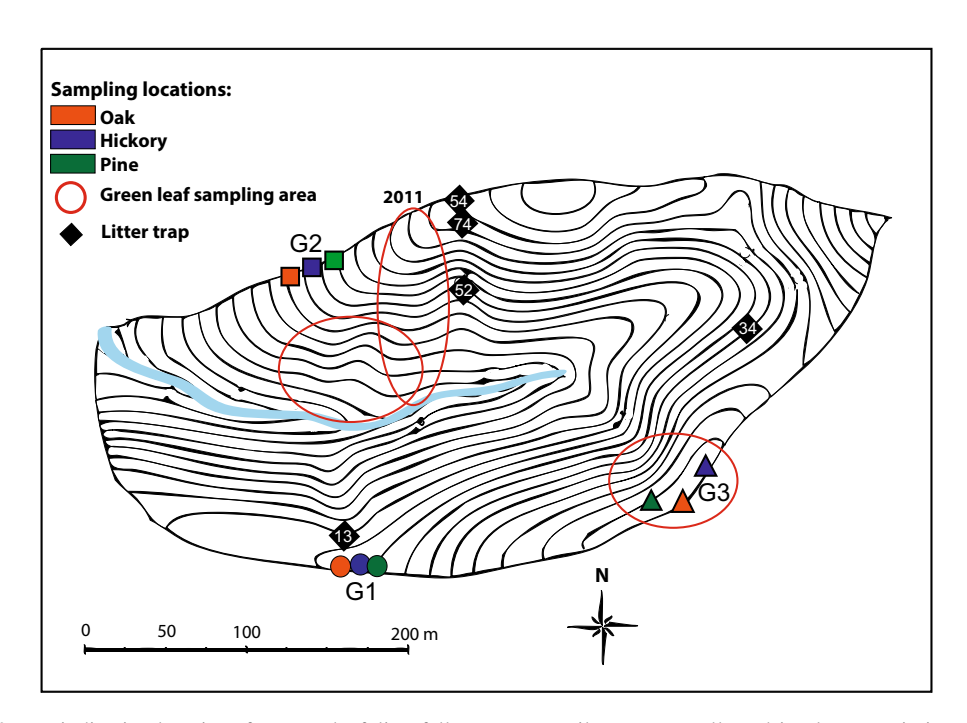


Fig. 1 SSHO map indicating locations for green leaf, litterfall, O horizon and soil core sampling. Litterfall was collected in litter traps. O horizon samples and soil cores were collected at the same ridgetop sites (G1, G2 and G3). At each ridgetop site,

one soil core was collected in close proximity to an oak (*red symbol*), hickory (*blue symbol*) or pine (*green symbol*) tree. The stream is denoted by a *blue line*. Contour interval is 2 m



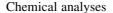
and pine (*P. virginiana* and *P. strobus*) species in summer 2009 and from sugar maples (*A. saccharum*) and chestnut oaks (*Q. prinus*) in summer 2011 by rope climbing and cutting down branches near the upper canopy of each tree. All samples were obtained between mid-June and mid-September. Samples collected in 2009 were obtained for each species at both valley floor and ridgetop locations (Wubbels 2010; Eissenstat et al. 2013; Kaye et al. 2015), while samples collected in 2011 were obtained along a planar transect on the north slope (Fig. 1).

Litterfall

Litterfall was collected in above-ground traps positioned 1 m above the land surface at five locations in the catchment, including the south slope swale ridge (trap 13), north slope swale ridge (traps 54 and 74), north slope swale midslope (trap 52), and south slope midslope near the eastern edge of the catchment (trap 34, see map Fig. 1). The leaves had no contact with the soil prior to collection. Litterfall was collected over a one week period in late summer (August 31, 2011), early autumn (October 3, 2011) and mid-autumn (October 31, 2011). The leaves collected in each trap were an assemblage from different tree species and the contribution of each species to the litterfall depended on the date of collection (Smith 2013; Kaye et al. 2016). Except in early October, oak leaves were the most abundant in the litterfall, reflecting the dominance of oaks in the watershed.

O horizon samples

O horizon samples (i.e., the organic material lying on the soil surface, d > 0 cm) were collected by hand at the ridge top sites G1, G2 and G3 in July 2012. The O horizons were thin (generally less than 5 cm thick) and consisted mostly of O_i material (i.e., partly decomposed leaves and needles). The O horizon also contained a small fraction of mineral material because, as is the case in most soils, the exact boundary between the O horizon and the A horizon was difficult to determine with precision; thus, the deeper part of the O horizon, which is close to the A horizon, was likely to contain some entrained mineral particles. All soil and organic samples were stored in plastic bags for transport to the laboratory.



Soil samples were covered with a paper towel to prevent contamination from the air and air-dried for one week in the laboratory. Dried soils were homogenized and split into subsamples using a riffle soil splitter. One subsample from each depth interval was ground with a ceramic mortar and pestle to pass a 150 µm sieve. For major element analysis, 100 mg of ground subsamples were fused with lithium metaborate at 900 °C for 10 min and dissolved in 5 % nitric acid. The resulting solutions were analyzed on an inductively coupled plasma atomic emission spectrophotometer (ICP-AES) at the Laboratory for Isotopes and Metals in the Environment (LIME) at The Pennsylvania State University. For trace metal analysis, ~ 100 mg of ground subsamples were completely digested in concentrated HF and HNO₃ acids and analyzed on an inductively coupled plasma mass spectrometer (ICP-MS) at Penn State LIME. Preparation blanks and a standard reference material (NIST2711) were analyzed in replicate.

O horizon, green leaf and litterfall samples were airdried and subsequently ground into a powder in liquid nitrogen using a mortar and pestle. The powdered samples were digested in 5 mL nitric acid (optima grade) in a microwave digester (MARS, CEM). The resulting acid digest was diluted to achieve a final nitric acid concentration of 5 % and analyzed by ICP-MS (Element 2, Fisher Scientific) at Princeton University. Elemental concentrations are reported on a dry weight basis.

Data processing

Soil cores

For each soil core and each element, we determined the mass transfer coefficient (τ_{ij}) as a function of depth. Mass transfer coefficients are defined for a mobile element j in weathered material/soil relative to a parent material and normalized to a relatively insoluble element i (Anderson et al. 2002; Brimhall and Dietrich 1987):

$$\tau_{ij} = \frac{C_{j,w}C_{i,p}}{C_{j,p}C_{i,w}} - 1,\tag{1}$$

where $C_{j,w}$ ($C_{i,w}$) and $C_{j,p}$ ($C_{i,p}$) represent the concentrations of the element j (i) in the weathered and parent materials, respectively.



In this study, we used Zr as the immobile element, following previous studies where Zr was identified to be present in the protolith as zircons (Jin et al. 2010; Herndon et al. 2011). The composition of the deepest soil sample was used as parent material for each core. Accordingly, all elements showed $\tau_{Zr,\ j}=0$ for the deepest soil sample, and deep leaching of elements from the true protolith, if applicable, could not be documented.

Positive mass transfer coefficients indicate a net addition of an element (j) to the soil profile relative to parent concentrations, while negative values indicate depletion relative to the immobile element (i) in the parent or protolith material. As a result, both atmospheric deposition and biological uplift result in positive mass transfer coefficients in the top soil layers, but biological uplift also creates negative mass transfer coefficients in the deep soil layers. Biogenic profiles may be difficult to identify if small depletions cannot be resolved within error.

For each element j, the average mass transfer coefficient in the A horizon was calculated as the average of the $\tau_{Zr, j}$ values in the upper 5 cm of the 9 soil cores.

Green leaves

Watershed-averaged elemental concentrations in green leaves (C(GL)) were calculated by multiplying elemental green leaf concentrations measured in SSHO tree species with the relative dominance of these tree species in the SSHO watershed as determined by Wubbels (2010) (Dataset DOI: 10.1594/IEDA/100268, Table S1).

Litterfall

With the notable exception of Al, and, to a lesser extent, Cr and Mo, elemental concentrations in litterfall showed limited variability across litter traps on a given date (Table S2). The collected leaf material was thus likely representative of litterfall in the watershed on that date. The average elemental concentrations in litterfall over the fall season, C(LF), were calculated from the elemental concentrations in litterfall at each collection date and weighted according to the contribution of the litterfall to the total litterfall mass (Table S2).

O horizons

Statistical analysis (Kruskal–Wallis test, 95 % confidence level) indicated that metal concentrations (with the possible exception of Al, see Table S3) were not significantly different in O horizon samples from oak, hickory and pine-dominated sites (Table S3). Thus, the O horizon was sufficiently well mixed to represent the entire watershed and did not reflect the dominant trees at the collection site. Concentrations measured at the 9 sites were therefore averaged to determine the average elemental concentration of the O horizon at ridgetop sites (C(O), Table 1).

Atmospheric, biological and soil production fluxes

Atmospheric deposition

In Table 2, we report annual atmospheric deposition fluxes at five urban and rural sites in New Jersey measured between July 1999 and January 2003 (NJ atmospheric deposition network). We also report annual deposition fluxes measured in southwestern Quebec (CA) over 2 years (1993–1995; Gelinas et al. 2000) and deposition fluxes measured in an urban and industrial area of NY and NJ (Yi et al. 2006). With the exception of Cd, the atmospheric deposition fluxes reported by Gelinas et al. (2000) are within the range of the NJ atmospheric deposition network, indicating that these fluxes can be assumed to be representative of the East Coast of the United States and Canada, at least in the 1990s. The fact that the deposition fluxes reported by Yi et al. 2006 are generally larger than those reported by either Gelinas et al. (2000) or the NJ deposition network is not surprising given that they were measured in heavily polluted areas. We chose the deposition fluxes reported by Gelinas et al. (2000) as an estimate for modern atmospheric deposition fluxes at the SSHO (F_{atm}, mg m⁻² year⁻¹).

Biological fluxes

For each metal, the annual biological flux due to addition of leaves to the land surface (F_{bio} , mg m⁻² year⁻¹) was calculated by multiplying the average metal concentrations in litterfall (C(LF), Table 1 and Table S2) with the annual production rate of litterfall normalized to land surface area ($F_{LF} = 380$ mg m⁻² year⁻¹, as determined by Smith (2013)):



Fable 1 Average element concentrations (dry weight basis, ± standard deviation) in green leaves [C(GL)], litterfall [C(LF)], O horizon [C(O)], A horizon [C(A)] and deep soil norizons ([C(deep)] and variable R describing metal retention in the O horizon. The deep soil horizons are defined here as the soil layers between the parent material (auger

Al (ppm)	Al (ppm)	P (ppm)	Fe (ppm)	Mn (ppm)	V (ppm)	Cr (ppm)	Co (ppm)	Cu (ppm)	Zn (ppm)	Mo (ppm)	Cd (ppm)
C(GL)	1,085 1,853 65	1,853	65	2,482	0.069	0.173	0.297 (0.082)	7.2	43	0.034	0.298 (0.068)
	(141)	(380)	(16)	(948)	(0.021)	(0.110)		(1.5)	(10)	(0.016)	
C(LF)	722	906	44	3,314	0.308	0.219	0.217 (0.105)	3	40	0.034	0.294
	(619)	(178)	(10)	(641)	(0.117)	(0.105)		(0.4)	(17)	(0.009)	(0.127)
	2,203	623	744	2,526	1.943	1.189	0.739 (0.253)	4	57	0.316	1.301
	(529)	(414)	(454)	(1,658)	(0.950)	(0.442)		(2)	(49)	(0.162)	(0.538)
	86,524	984	46,108	4,397	128	78	20	31	117	1.43	0.39
	(4,064)	(234)	(3,714)	(3,610)	(14)	(10)	(3)	(20)	(22)	(0.47)	(0.18)
	100,284	773	51,752	2,009	147	91	22	38	105	0.89	0.22
	(4,750)	(132)	(4,145)	(1,172)	(6)	(9)	(3)	(26)	(17)	(0.27)	(0.059)
0	0.025	0.633	0.016	0.574	0.015	0.015	0.037	0.133	0.487	0.221	3.359
R, if $f = 0.015$	1.3	0.67	pu	0.74	pu	pu	2.0	1.0	1.4	8.7	4.4
	+ 0.7	+ 0.46		+ 0 51			¢ + +	+ 0.7	+ 1	4 4 8	+ 1 9



Soil production fluxes

The soil production fluxes (resulting from the transformation of deeper soil into A-horizon soil, $F_{\rm soil}$, mg m $^{-2}$ -year $^{-1}$) were calculated by multiplying the average metal concentration in the soil below the A horizon at the 9 ridgetop sites (C_{deep}, Table 1) with average soil bulk density ($\rho=0.96$; Lin et al. 2006) and the soil production rate at the ridgetop (ω), which was previously estimated to be $\omega=45$ m My $^{-1}$ (Ma et al. 2011):

$$F_{\text{soil}} = C_{\text{deep}} \times \rho \times \omega.$$
 (3)

Metal residence times in the A horizon

The average residence times of elements in the A horizon at each ridgetop site were calculated with a one-box model representing the A horizon (top soil layer, -5 cm < d < 0, Table 3). For each metal, the mass per unit area of a metal in the A horizon $(m_j(A))$ was calculated from the metal concentration in the A horizon $(C_i(A))$, see Tables 1 and S5) as:

$$m_i(A) = C_i(A) \times \rho \times d,$$
 (4)

with depth d=5 cm, $\rho=0.96~g\text{ cm}^{-3}$ (Lin et al. 2006). The residence time (RT) for each element in the upper 5 cm of soil was calculated as:

$$RT = m_j(A)/(F_{bio} + F_{atm} + F_{soil}).$$
 (5)

For this calculation, we assumed that the A horizon is currently at steady state with respect to its metal concentrations. It is only a preliminary estimate as it does not take into account intra-annual variability or long-term variations. Long term variations may arise if soil concentrations are adjusting to reduced atmospheric deposition fluxes corresponding to reduced industrial activities in Pennsylvania over the last half-century (Herndon and Brantley 2011). In addition, these average residence times do not account for the fact that metals may partition in pools with different residence times.

Statistical analyses

All statistical analyses were carried out in MATLAB. Statistical analysis of the variations of elemental mass



Table 2 Comparison of current atmospheric deposition fluxes, biological element fluxes (Fbio) and soil production fluxes (Fsoil) reported as mg m⁻² year⁻¹

	Al	Ь	Fe	Mn	Λ	Cr	Co	Cu	Zn	Mo	Cd
Atmospheric deposition Gelinas et al. 2000 (F_{dm}) \pm	37.3 (12.6)	pu	36.5 (11.4)	5.03 (2.35)	0.38 (0.14)	0.23 (0.07)	0.063 (0.023)	1.19 (0.31)	14 (4.6)	0.039 (0.011)	0.270 (0.08)
Atmospheric deposition NJ atm dep net	24–56	5.2-8.1	23–87	1.9–3.4	0.4-1.1	0.056 - 0.3	0.03 - 0.16	0.49 - 2.2	5.5-12	pu	0.023-0.08
Atmospheric deposition Yi et al. 2006	383-730	pu	pu	11–16	0.7–3	3.6-5.1	pu	4-13	14–51	0.03 - 0.15	0.01 - 0.05
Biological flux (Fbio)	274	344	17	1,259	0.117	0.083	0.082	1.3	15	0.013	0.11
Soil production flux (F _{soil})	4,500	35	2,300	06	9.9	4.1	1.0	1.7	4.7	0.04	0.01

Table 3 Average residence times (years ± standard deviation) of elements in the A horizon at the ridgetop sites G1, G2 and G3

Site	Al	Ь	Fe	Mn	Λ	Cr	Co	Cu	Zn	Mo	Cd
G1 ±	925 (62)	92 (9)	935 (36)	(8)	1,000 (115)	1,027 (83)	883 (107)	64 (6)	329 (39)	475 (74)	36 (3)
G2 ±	892 (26)	154 (7)	1,031 (115)	230 (72)	870 (44)	797 (35)	977 (24)	123 (84)	314 (55)	986 (110)	70 (30)
G3 ±	874 (23)	135 (23)	938 (31)	190 (210)	838 (26)	844 (28)	779 (181)	68 (35)	291 (91)	878 (172)	43 (14)



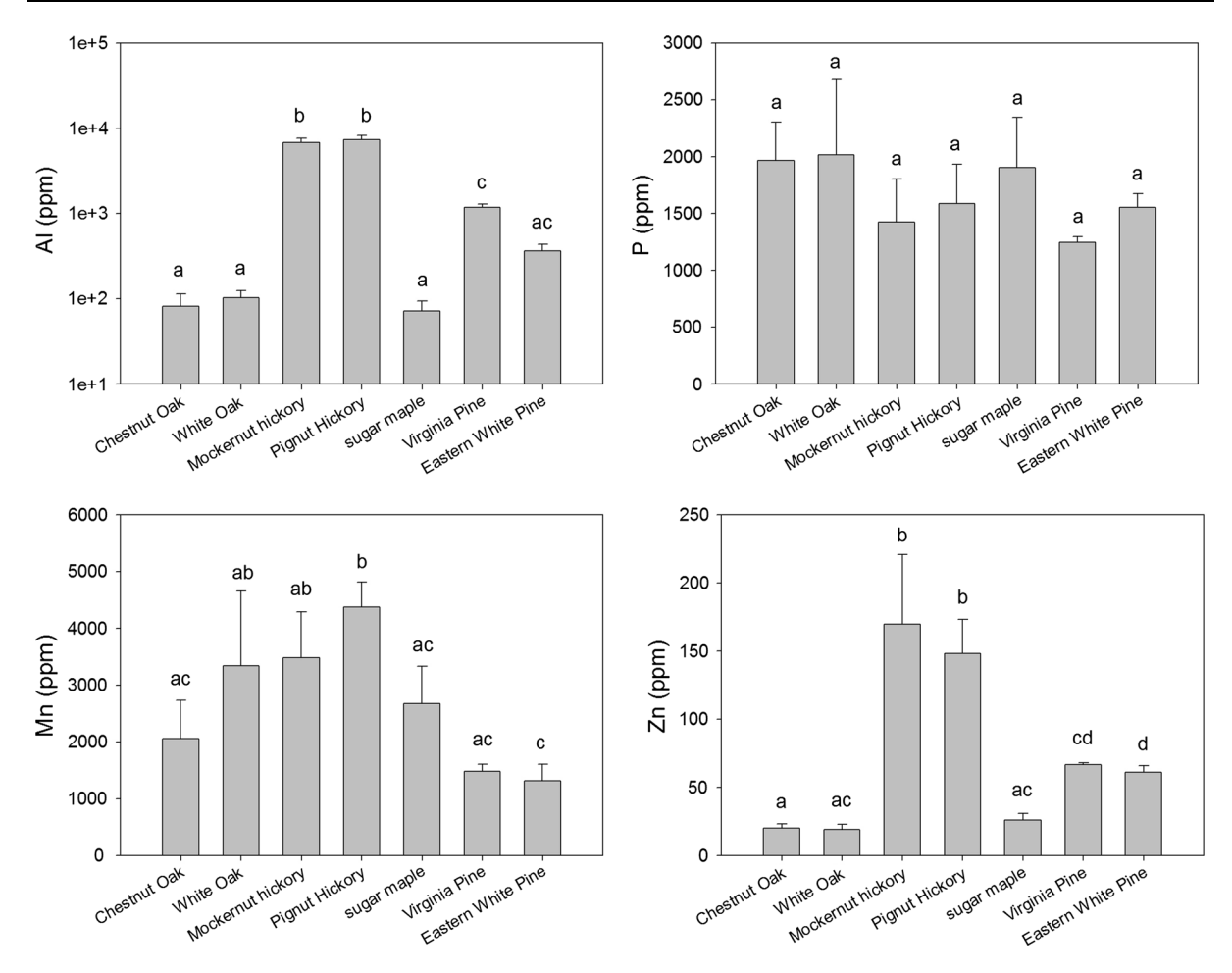


Fig. 2 Elemental concentrations (dry weight basis) in green leaves of representative tree species growing in the SSHO watershed collected in the late spring to late summer of 2011

transfer coefficients within collection site, depth and dominant vegetation types was carried out with a linear Mixed-effects model (p < 0.05). One-way ANOVA tests (p < 0.05) were used to analyze: 1-the variations in the metal composition of the O horizon with vegetation type and 2-the variations in metal composition of green leaves across tree species. Kruskal–Wallis tests (p < 0.05) were used to determine the variability of metal concentrations in the O horizon across collection sites.

Results and discussion

Metal concentrations in green (canopy) leaves

Concentrations of certain elements (P, Fe, V, Cr, Mo, Cu) in mature green leaves showed little variation

(Note the logarithmic scale for Al). Error bars correspond to standard deviations. Bars labeled with different letters have significantly different means (ANOVA test, 95 % confidence level)

across tree species (Fig. 2, Table S1). In contrast, other elements (Al, Co, Zn, Cd), and to a lesser extent, Mn, were more variable and more concentrated in the green leaves of hickory species. The largest variations in concentrations across tree species were observed for Al, with concentrations in hickory leaves almost two orders of magnitude greater than in oak leaves. Aluminum, Co, Zn and Cd concentrations in green leaves were highly correlated ($r^2 > 0.79$, r = 39).

Elemental leaf concentrations were not expected to directly reflect soil concentrations since plant elemental uptake is affected by element bioavailability and plant homeostasis. Nonetheless, on a log-log plot of the watershed-averaged metal concentrations in green leaves (C(GL)) versus the average concentration in the A horizon (C(A)), elements approximately fell on two distinct lines-high uptake and low uptake that indicate



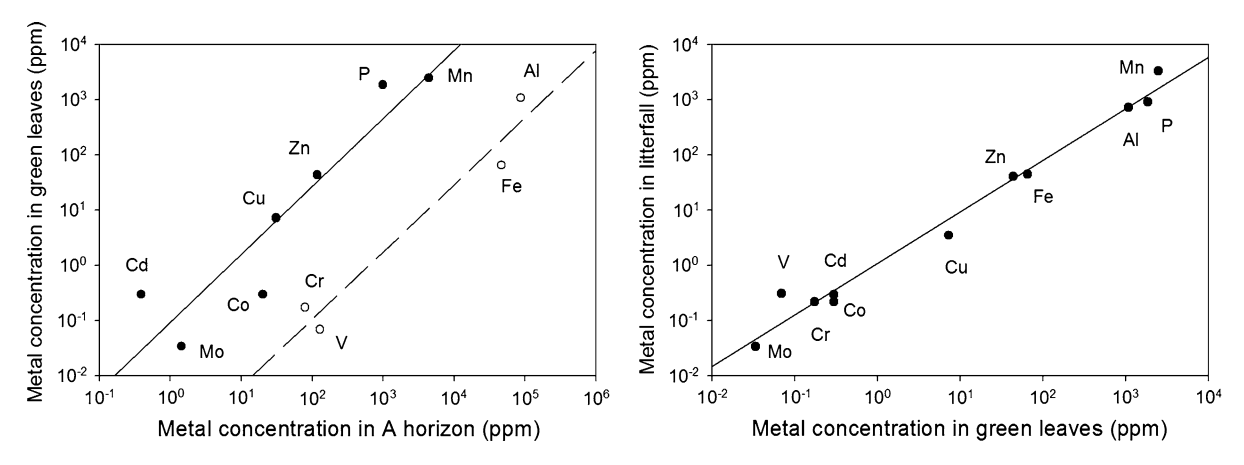


Fig. 3 Left panel Relationship between metal concentrations in green leaves and in the A horizon. Right panel Relationship between metal concentrations in litterfall and in green leaves

a general correlation between green leaf concentrations and soil concentrations (Fig. 3). Most elements (Mo, Cd, Co, Cu, Zn, P and Mn) fell on the high uptake line. Four metals: Al, Fe, Cr and V, fell on the low uptake line, with leaf concentrations approximately two to three orders of magnitude less than predicted from their soil concentrations if they had been on the high uptake line. Interestingly, these four metals also exhibited similar soil concentration profiles, which showed a conservative behavior (see below). Mn concentrations in green leaves were higher than all other elements considered in this study. Indeed, Mn concentrations in leaves were two to three orders of magnitude larger than concentrations required for photosynthetic growth (Raven 1990). Mn concentrations were even greater than that of phosphorus, in spite of lower biological requirements for Mn. Green leaf Mn concentrations were also higher than Fe and Al, which were present in much higher concentrations in soils, but fell on the low uptake line.

Interestingly, Cd, which is toxic, fell on the high uptake line with essential nutrients like P, Cu and Zn. This may reflect the intrinsic difficulty for plant metal uptake systems to take up essential elements like Mn and Zn while discriminating against Cd, which has a very similar chemistry (Sunda and Huntsman 1996; Xu and Morel 2013). Alternatively, Cd may have a yet-to-be discovered biological role in plants, possibly similar to its role as a metal cofactor in carbonic anhydrases in marine algae (Xu et al. 2008).

Metal concentrations and retention in litterfall and O horizon

Watershed-averaged metal concentrations in litterfall reflected primarily metal concentrations in green leaves (Fig. 3). The influence of resorption (or accretion) processes, which tend to decrease (or increase) elemental concentrations in leaves during leaf senescence, appeared to be minor (except possibly for V), and cannot be resolved within the uncertainties of our dataset.

Unlike the other soil horizons, O horizons have a relatively short turnover time on the order of a few years and elemental concentrations change as organic material is decomposed. Decomposition, which decreases leaf mass mainly through loss of carbon by respiration, tends to increase metal concentrations (in wt %) in the O horizon, while leaching of metals decreases their concentrations in the O horizon. The balance of these two processes determines whether metal concentrations increase or decrease in the O horizon over the course of a year. To evaluate the role of organic matter in elemental cycling at the SSHO, we examined how organic matter binds to metals and retains them near the soil surface. We thus compared elemental concentrations in the litterfall (collected in the fall of 2011) and in O horizon samples (collected the following summer). Phosphorus concentrations were lower in the O horizon than in litterfall. In contrast, all metals were either similar or enriched in the O horizon compared to litterfall (Table 1). Fe, V, Cr and Mo were strongly enriched (between 5 and 17 times) in the O horizon



relative to leaf litter. Differences in element concentrations between the litterfall and the O horizon may reflect changes in the composition of plant-derived organic matter as it decays on the forest floor; however, changing concentrations may also reflect mixing of organic matter with mineral phases entrained from the A horizon. To untangle the importance of these two processes, we developed a simple model where we described the O horizon as a mixture of organic material (decaying leaves and more humified organic material) and some (presumably small) fraction of mineral soil. The contribution of atmospheric deposition and throughfall to phosphorus and metal concentrations is considered to be negligible during the relatively short time that the leaves spend on the ground as leaf litter.

Using this approach, the mass per unit area of the O horizon $(M_O, g m^{-2})$ was calculated as:

$$M_O = M_{OM} + M_{Min}. (6)$$

Here, M_{OM} and M_{Min} are the mass per unit area (g m⁻²) of organic material and minerals, respectively, in the O horizon. The concentration of a given metal (j) in the O horizon ($C_i(O)$) is thus:

$$C_j(O) = \frac{M_{OM}C_j(OM) + M_{Min}C_j(A)}{M_O}, \tag{7}$$

where $C_j(OM)$ and $C_j(A)$ are the concentrations of the element j in the organic fraction and the mineral fraction, respectively. We assumed that the mineral fraction in the O horizon has the same elemental composition as the A horizon. Rearranging Eq. (7) yields:

$$C_j(O) = \frac{M_{OM}}{M_O} C_j(OM) + \frac{M_{Min}}{M_O} C_j(A).$$
 (8)

We define $f = \frac{M_{Min}}{M_O}$, which represents the fraction of mineral material present in the O horizon and is the same for all elements.

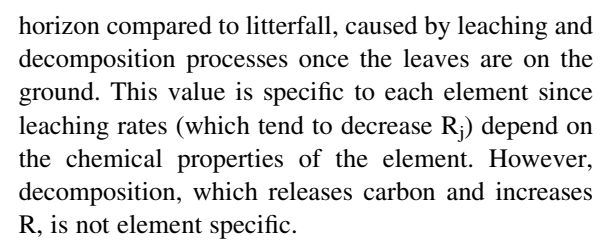
Substituting f into Eq. (6) implies that:

$$\frac{M_{OM}}{M_O} = 1 - f. \tag{9}$$

We also define a "metal retention parameter" R_i:

$$R_j = \frac{C_j(OM)}{C_j(LF)},\tag{10}$$

where C_j (*LF*) is the concentration of j in litterfall. R_j represents the enrichment (if $R_j > 1$) or depletion (if $R_j < 1$) of element j in the organic fraction of the O



Equation (8) can now be re-written as:

$$C_i(O) = (1 - f)R_iC_i(LF) + fC_i(A).$$
 (11)

We observed that the concentrations of Fe, V and Cr in litterfall were small compared to the concentrations of these elements in the A horizon (Table 1). Assuming that R_i is small for these metals, and recognizing that (1-f) is always less than 1, the contribution of Fe, V, and Cr in the mineral fraction is likely to be dominant over that of the organic fraction for these metals. Consistent with this argument, we calculated $f = 0.015 \pm 0.001$ using Eq. (11) and concentration data for Fe, V and Cr (Table 1). The fact that all three metals provided a similar value for f is consistent with the inference that the mineral fraction dominates O horizon concentrations for these metals. Substituting this value of f = 0.015 into Eq. (11), we then calculated the metal retention parameter in the O horizon (R_i) for the other metals. The values of R_i provided a relative measure for the retention of each metal by organic matter in the O horizon, with high R_i values indicating strong retention due to a large affinity of the metal for NOM or the formation of immobile mineral phases (Table 1).

Phosphorus, Mn, Al, Co, Cu and Zn showed intermediate retention in the O horizon (R_i close to 1). In contrast, Mo and, to a lesser extent, Cd were significantly enriched in the organic fraction of the O horizon compared to litterfall (large R_i), indicating slow leaching rates for these two elements. This analysis showed that elements in the O horizon fell into three groups: 1-elements whose O horizon concentrations were dominated by a small but significant contribution of minerals entrained from the A horizon (Fe, V and Cr); 2-elements whose concentrations in the organic fraction of the O horizon were similar to their concentrations in litterfall (P, Mn, Al, Co, Cu and Zn) and 3-elements whose concentrations in the organic fraction of the O horizon were significantly enriched compared to the litterfall (Mo and Cd).



Mass transfer coefficients

Mass transfer coefficients ($\tau_{Zr,j}$ values) were calculated as a function of soil depth for for each element in the nine ridgetop soil cores (Fig. 4). All elements except for Cr, Cu and V had $\tau_{Zr,j}$ values that varied significantly with depth (Mixed-effects model, 95 % confidence level). Phosphorus, Mn, Mo and Cd showed a strong enrichment $(\tau_{Zr,j} > 0)$ in the A horizon. Of all metals, Mn demonstrated the largest $\tau_{Zr,i}$ values near the soil surface. Depending on the site, Cu and Co showed either a small enrichment ($\tau > 0$) or a small depletion ($\tau < 0$) in the A horizon. Aluminum, Fe, V and Cr showed a distinct behavior, with slightly decreasing (negative) $\tau_{Zr,i}$ values towards the surface, consistent with depletion relative to Zr and the parent concentration (Fig. 4 and Table S4). Pairwise comparisons showed that the $\tau_{Zr,j}$ values for these four metals are correlated ($r^2 > 0.5$, n = 60). Vanadium and Cr had the highest correlation coefficient $(r^2 = 0.91, n = 60)$, suggesting similar soil cycling for these metals.

The $\tau_{Zr,j}$ values for Fe, Al, Cr, Mn, Mo and V were significantly different across collection sites (i.e., G1, G2 or G3, Mixed-effects model, 95 % confidence level). The dominant vegetation type (i.e., pine, oak or hickory) had a significant effect on the $\tau_{Zr,j}$ values of Al, Co, Cu, Mn, Mo and P (Mixed-effects model, 95 % confidence level).

Consistent enrichment at all depths compared to the bottom-most sample (i.e., $\tau_{Zr,j} > 0$) was observed for P, Mn, Cu, Zn, Mo, Cd and might reflect: 1-atmospheric deposition that added the metal to the soil; 2-upward biological mobilization from bedrock and re-deposition near the surface. Either of these two metal sources (atmospheric inputs or bedrock) may cause enrichment at the surface that can then be exacerbated by strong binding of metals to NOM, adsorption on mineral surfaces, or, for metals such as Mn and Fe, precipitation of oxide minerals. Such processes would result in low leaching rates and a long residence time. In contrast, consistent depletion of an element over the entire soil profile $(\tau < 0)$, as observed for Al, Fe, V and Cr, can result from physical and/or chemical weathering losses (Brantley and White 2009).

Metal accumulation in the top soil layer (A horizon, upper 5 cm of soil)

Enrichment was observed in the A horizon (upper 5 cm of soil) ($\tau > 0$) for a number of metals (i.e., Mn,

Cu, Zn, Mo, Cd). As shown in Fig. 5, which illustrates how elements cycle through soil and vegetation at the SSHO, the sources of metals into the A horizon were: 1-atmospherically-derived metals; 2-metals cycled through vegetation and redeposited as litterfall or throughfall (note that for this mechanism, the metal could be derived originally either from bedrock or from previous atmospheric inputs into the soil); 3-transformation of soil from horizons at depth into A horizon material.

Atmospheric fluxes

Modern atmospheric deposition fluxes at the SSHO (F_{atm}, mg m⁻² year⁻¹) were assumed to be similar to the fluxes reported in the Gelinas et al. study (Gelinas et al. 2000) in Southwestern Quebec (Canada, see Methods and Table 2). As shown in Fig. 6, atmospheric deposition fluxes and A horizon concentrations were generally correlated. In particular, Al, Fe, Mn, V, Cr, Co and Mo fell along a line on a log-log plot, with Al and Fe showing the largest A horizon concentrations and atmospheric fluxes. The observed correlation could in principle reflect the fact that large atmospheric deposition fluxes resulted in large soil concentrations. However, as detailed below, the magnitude of the atmospheric flux was too small to significantly affect soil concentrations for Al, Fe, Cr, V and Co. For this reason, the observed correlation most likely reflects the fact that the bulk atmospheric deposition measured in the Gelinas et al. study included soil particles with metal concentrations broadly similar to the SSHO soils. Interestingly, Cu, Zn, and Cd fell outside this general correlation, with larger deposition fluxes than expected compared to the other elements. This presumably reflects a large direct anthropogenic contribution to deposition fluxes for these metals.

Biological fluxes

Biological fluxes for each metal (F_{bio} , mg m $^{-2}$ ·year $^{-1}$) were calculated by multiplying the average metal concentration in litterfall with the annual rate of litterfall production (see "Materials and methods" section). Of all the elements considered, Mn had the largest biological flux, followed by P and Al (Table 2). This reflected the large Mn, P and Al concentrations in litterfall, which in turn reflected concentrations in mature green leaves (Fig. 3).



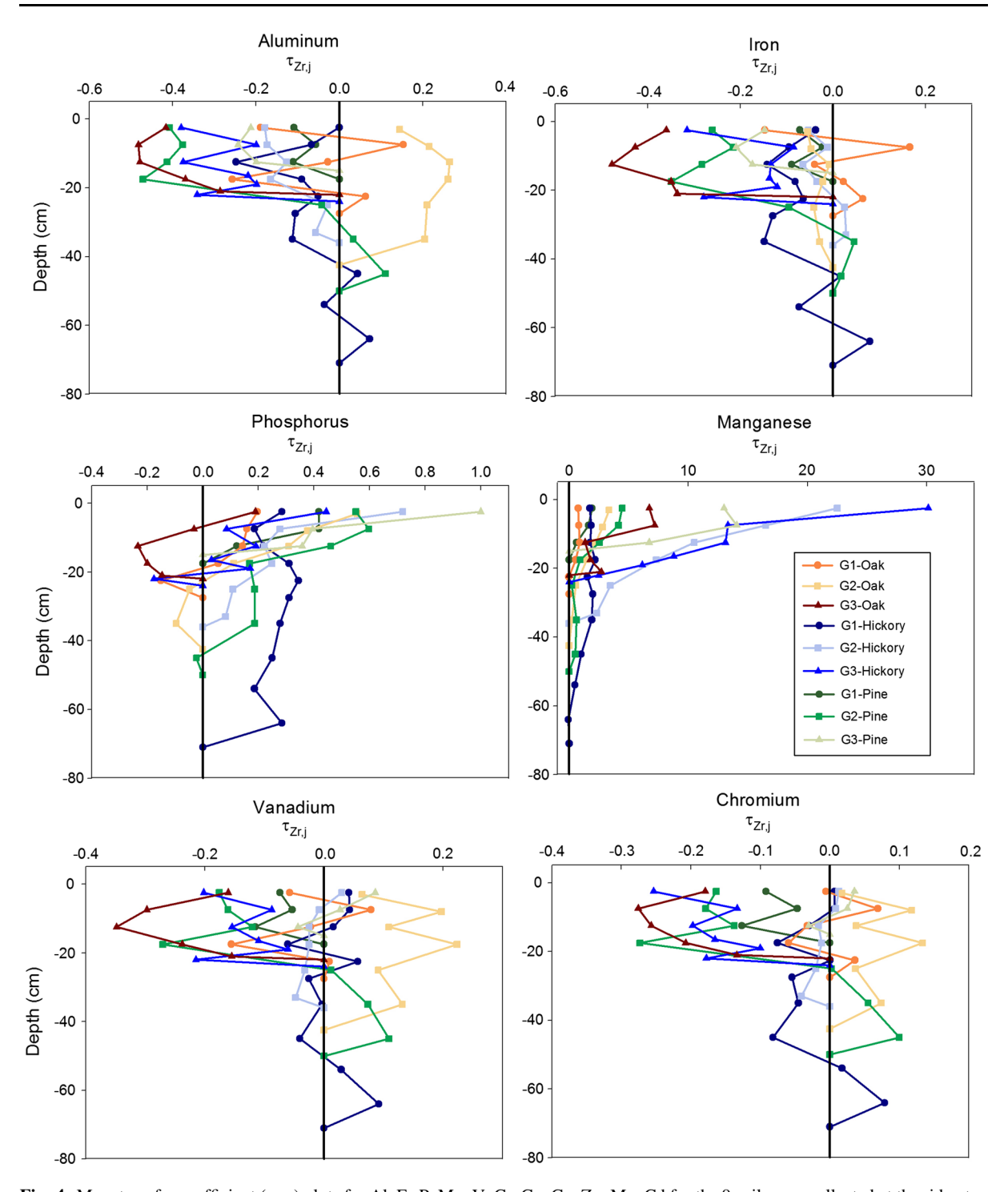


Fig. 4 Mass transfer coefficient $(\tau_{Zr,j})$ plots for Al, Fe P, Mn, V, Cr, Co, Cu, Zn, Mo, Cd for the 9 soil cores collected at the ridge top sites G1, G2 and G3 (see Fig. 1). The top of the A horizon is defined as d=0 cm



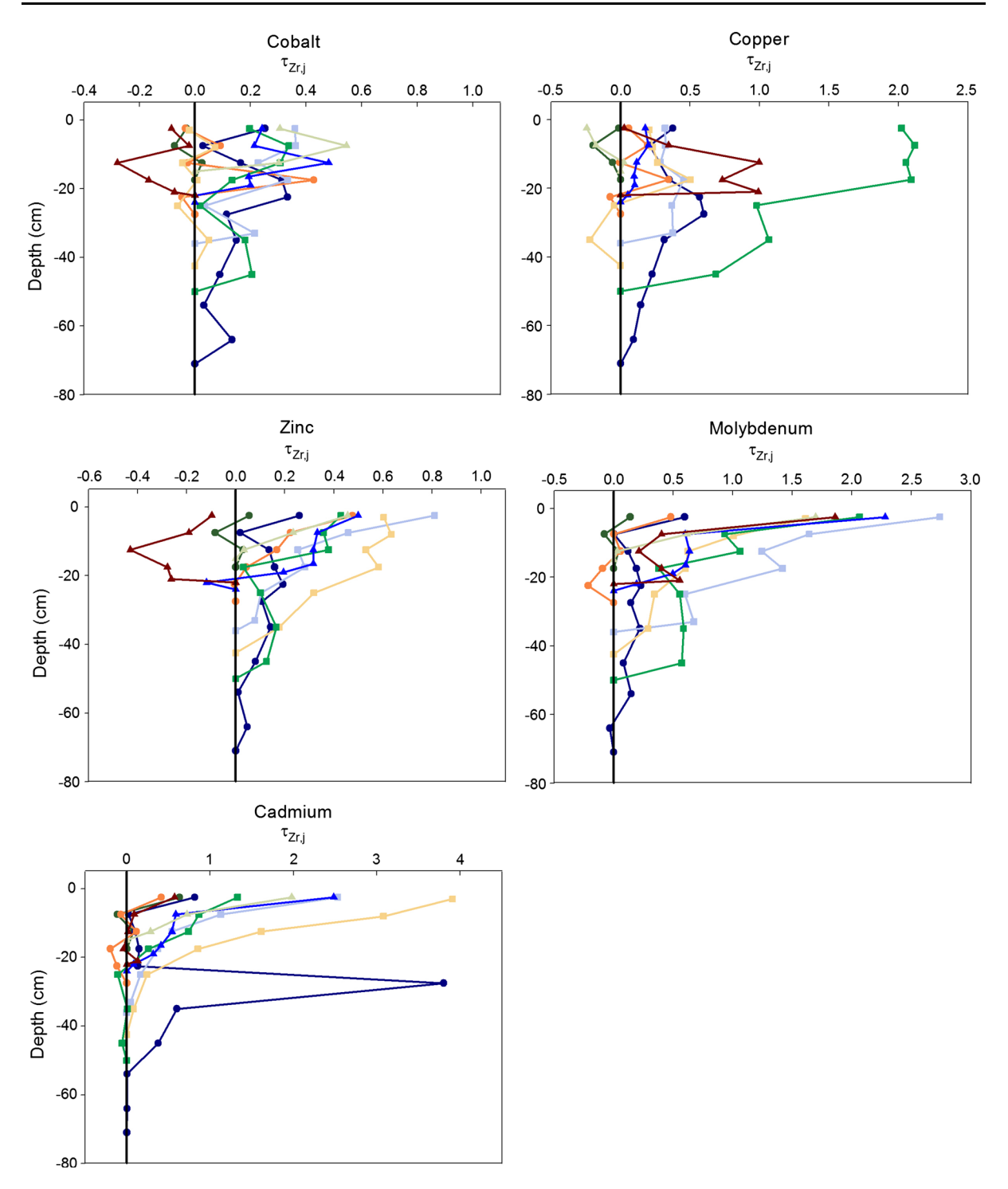


Fig. 4 continued

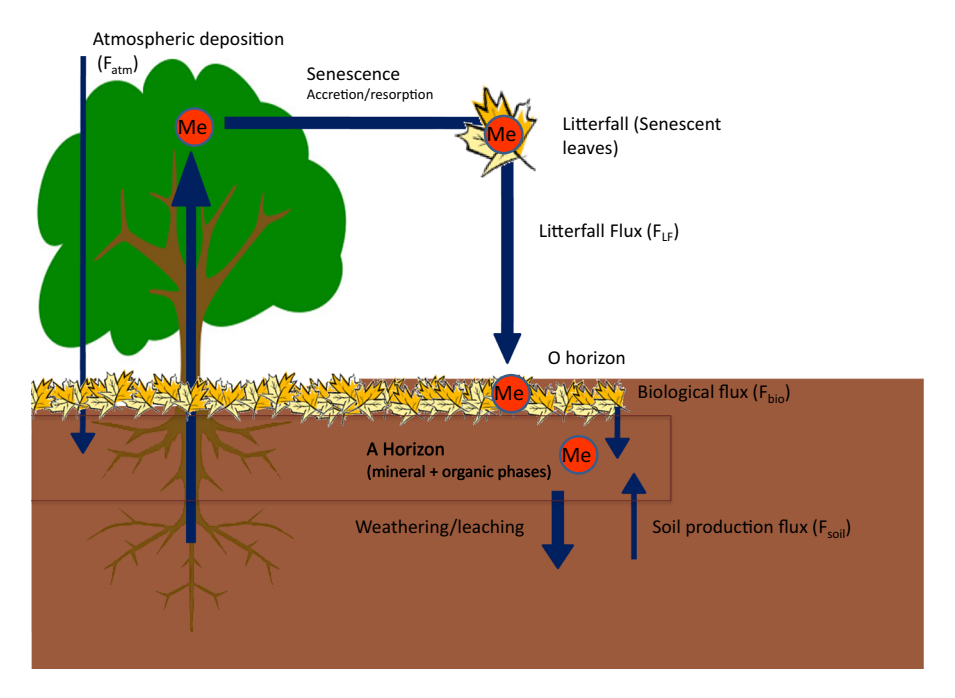


Fig. 5 Conceptual diagram of metal cycling in soils at SSHO

Soil production fluxes

The soil production fluxes (F_{soil} , mg m⁻² year⁻¹) were calculated by multiplying the average metal concentrations below the A horizon with the soil production rate at the SSHO (see "Materials and methods" section). Aluminum and Fe had the largest soil production fluxes, followed by Mn and P (Table 2). The relative magnitude of these fluxes directly reflects the elemental abundance in the SSHO soils.

Metal enrichment in the A horizon

Large surface inputs (i.e., atmospheric and biological fluxes) tend to increase τ near the soil surface while steady upward movement of soil particles that experience minimal chemical weathering create uniform τ profiles with depth. To quantify the relative importance of these fluxes, we defined F_{ratio} as the ratio of surface fluxes (atmospheric deposition and biological uplift) to soil production fluxes:

$$F_{\text{ratio}} = (F_{\text{atm}} + F_{\text{bio}}) / F_{\text{soil}}. \tag{12}$$

A plot of F_{ratio} as a function of the average mass transfer coefficient in the A horizon for each metal showed the expected relationship, with larger τ values corresponding to larger F_{ratios} (Fig. 7). Two metals,

Mn and Mo, fell outside the general correlation. In addition to a large $F_{\rm ratio}$, strong binding to NOM and adsorption to mineral surfaces, both of which retain metals in the top soil layer, tend to maintain any increase in $\tau_{\rm Zr,i}$ near the soil surface.

Metals fell into three categories

- (a) Al, Fe, V, Co and Cr (conservative elements). These metals had a low F_{ratio} because soil production fluxes were dominant over surface inputs. Accordingly, they showed low (slightly negative to slightly positive) $\tau_{Zr,j}$ values in the A horizon (Figs. 4, 7). The soil profiles for these metals were likely dominated by geological processes with little detectable influence of biology or external inputs through atmospheric deposition. In general, these metals were conservative within the soil or slightly lost from the soil when considered over the entire soil depth.
- (b) P, Cu, Zn and Cd (enriched elements). These elements had large F_{ratio} (F > 1) and were enriched in the A horizon relative to parent material ($\tau_{Zr,j} > 0$) (Fig. 7). We infer from the observed positive correlation between F_{ratio} and $\tau_{Zr,j}$ that elevated biological and/or atmospheric



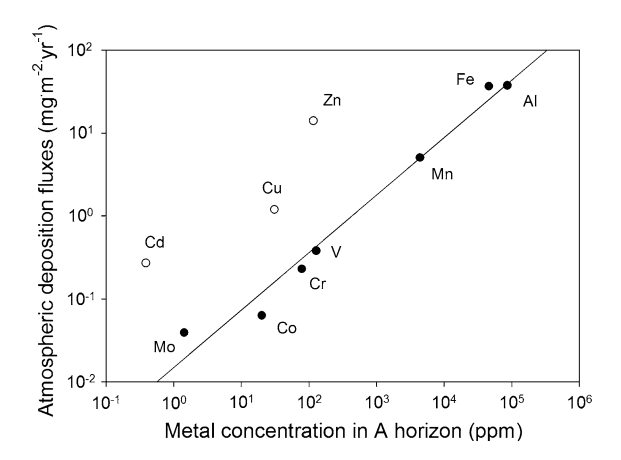


Fig. 6 Relationship between metal atmospheric deposition fluxes and concentrations in the A horizon

inputs generate surface enrichment. The largest surface inputs of P are associated with biological fluxes (F_{bio}) whereas biological (F_{bio}) and atmospheric fluxes (F_{atm}) are comparable for Cu, Zn and Cd (Table 2).

(c) Mn and Mo (retained elements). Mn and Mo had positive $\tau_{Zr,j}$ values over the entire soil column and were clear outliers in the relationship between F_{ratio} and $\tau_{Zr,j}$ values shown in Fig. 7. Both metals showed higher $\tau_{Zr,j}$ values than expected based on their F_{ratio} . The biological flux for Mn, unlike that for Mo, was large and accounted for most of the modern surface input. Interestingly, the largest $\tau_{Zr,j}$ values for Mn were measured at hickory-dominated sites (Fig. 4)

that also exhibited the highest Mn concentrations in green leaves. Nonetheless, the comparison of Mn with P shows that neither this large biological flux nor a strong retention by NOM can account for the large $\tau_{Zr,j}$ values for Mn. Specifically, Mn and P have a similar F_{ratio}, and similar retention by NOM (as shown by the values of R_i), but the $\tau_{Zr,j}$ value for Mn in the A horizon was much larger than that for P. It is thus possible that Mn enrichment in the A horizon reflects a refractory pool of Mn originating from past atmospheric deposition due to steel emissions and coal burning in Pennsylvania (Herndon et al. 2011; Ma et al. 2015). Additionally, leaching of Mn from the soil profile may be inhibited relative to P due to its unique redox properties. Mn(II) stored in leaves is rapidly oxidized to Mn(IV) and precipitates as Mn-oxides during litter decomposition (Lytle et al. 1996; Fernando et al. 2010; Herndon et al. 2014). External inputs of Mn combined with slow leaching rates may account for the high Mn $\tau_{Zr,i}$ values.

After Mn, the second largest $\tau_{Zr,j}$ values in the A horizon were observed for Mo despite its relatively small F_{ratio} . The biological flux for Mo was very small while modern atmospheric deposition and soil production fluxes were similar in magnitude. Like Mn, the large $\tau_{Zr,j}$ values for Mo may reflect in part an old and refractory anthropogenic Mo pool (Meij and Winkel 2007, Querol et al. 2007). This interpretation is consistent with a recent study by Chappaz et al. (2012)

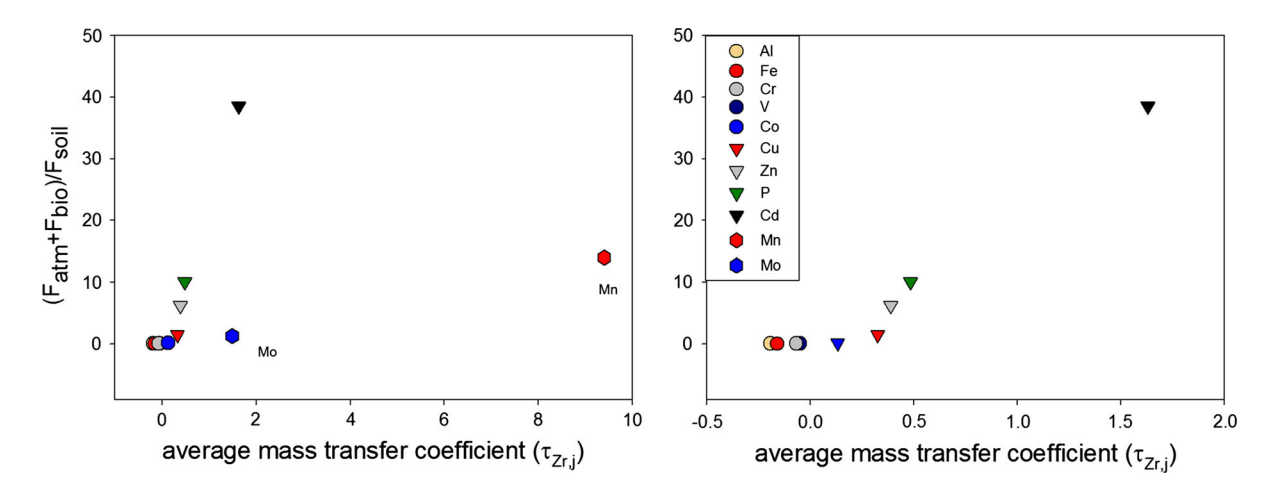


Fig. 7 Left panel Relationship between the mass transfer coefficients in the A horizon (averaged across soil cores for each element) and ratios of surface inputs to the soil production flux: $F_{ratio} = (F_{atm} + F_{bio})/F_{soil}$. Right panel same as left panel without Mn and Mo



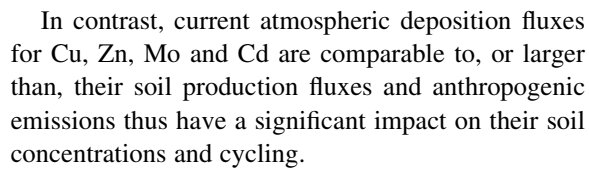
showing a large anthropogenic contribution to Mo deposition in sediments in Eastern Canada from fossil fuel burning and smelting activities. The retention of Mo in the A horizon, as shown by the large $\tau_{\text{Zr},j}$ values, is also interesting in view of its unusual chemistry. Unlike most transition metals, aqueous Mo in oxic environments is in the form of a negatively charged ion, molybdate (MoO₄²⁻). Molybdate is highly soluble in pH-neutral or basic environments, but the low pH of the SSHO soils (pH \sim 4, Jin et al. 2010) favors the adsorption of the negatively charged molybdate on mineral surfaces, thereby favoring its retention in the A horizon (Dzombak and Morel 1990). In contrast, the positively charged metals Co, Cu, Zn and Cd are expected to adsorb only weakly to mineral surfaces at this low pH. Mo enrichment in the A horizon may also reflect its strong affinity for NOM, as shown in previous studies (Wichard et al. 2009; Wurzburger et al. 2012) and indicated here by its large R_{Mo} value.

Metal residence times in the A horizon

Al, Fe, V, Cr and Co have long residence times similar to the residence time of soil in the A horizon (\sim 1,000 years), as expected since their cycling is controlled primarily by soil production and erosion processes (Table 3). The residence time of Mo is also very long, most likely reflecting the strong interaction of Mo with NOM and mineral surfaces (large R_{Mo}). Zinc, Cu, Mn, P and Cd may have shorter residence times, ranging from several decades to several centuries, depending on the element and the sampling site. Zinc has a longer residence time than Cu and Cd, reflecting its larger soil concentration. These calculated residence times are within the ranges of values reported by Alloway (1995).

Impact of anthropogenic inputs on soil concentrations

For some metals (i.e., Al, Fe, Mn, V, Cr, Co), current atmospheric deposition fluxes are typically less than 10 % of the soil production fluxes, suggesting that the present impact of human activities on the soil cycle of these metals is small (Table 2). Nonetheless, anthropogenic contributions for these metals (particularly Mn) in the past may have been significantly higher and their remnants may still affect soil concentrations due to their long residence time.



The large atmospheric deposition fluxes of Cu and Cd are of particular concern, considering their well-documented toxicity for microorganisms.

In view of the low Mo levels in the soil, Mo toxicity effects on soil biota and plants are unlikely. Nonetheless, because atmospheric deposition fluxes are comparable to soil production fluxes, and considering the strong binding of Mo to NOM, it appears likely that Mo concentration in the A horizon, and thus the Mo cycle in these soils, have been strongly affected by human activities. This raises the possibility that Mo limitation of nitrogen fixation, which has been observed in natural and managed ecosystems (e.g., Gupta 1997, Wurzburger et al. 2012), might be less severe today than it was in the past, at least in these soils.

It is worth noting that the persistence of anthropogenic metals in the soil can be exacerbated by the vegetation, which either creates a large biological flux that takes up the metal from the deep soil layers and brings it back to the soil surface (as is the case for Mn) or provides a source of NOM which binds the metal strongly and reduces its leaching out of the soil (as is the case for Mo). The metals for which anthropogenic inputs are likely to have the most lasting influence are those with atmospheric fluxes that contribute significantly to the inputs and which have a long residence time in the soil. Based on the results of our study those are: Mn, Mo and to a lesser extent, Cu, Zn and Cd.

Conclusions

The O and A horizons are the two loci in the soil that store most of the chemical energy in the form of photosynthetically fixed carbon. This energy is available to fungal and bacterial communities that actively recycle nutrients in the soil. Changes in metal bioavailability in these horizons may affect microbial activity and, ultimately, the cycling of major soil nutrients such as carbon and nitrogen. An integrated approach, looking at both the soil and the vegetation in the SSHO watershed, revealed some of the mechanisms responsible for metal enrichment often observed



in the O and A horizons. Elemental concentrations in the O horizon were controlled by the organic matter (mainly decomposing litterfall) and a small but significant fraction of mineral phases entrained from the A horizon. Iron, V, Cr and Mo were highly enriched in the O horizon compared to the litterfall. The mineral fraction was responsible for the observed enrichment for Fe, V and Cr in the O horizon. In contrast, Mo enrichment largely reflected strong retention of Mo by NOM in the O horizon.

In the A horizon, P, Cu, Zn and Cd showed significant enrichment compared to deeper soil horizons due to both biological uplift and atmospheric deposition. Manganese and Mo were the two most strongly retained metals, with concentrations that are difficult to account for based on current input fluxes. The observed enrichment most likely reflects the unusual chemistry of these two metals as well as large anthropogenic deposition fluxes in the past. This study outlines the critical role played by vegetation in redistributing metals across the soil profile. It also highlights the far-reaching influence of vegetation on the chemical speciation of metals, and thus on their bioavailability and transport properties. An integrated approach accounting for the tight interplay between the soil and the vegetation is necessary to understand elemental cycling in soils.

Acknowledgments This study was supported by National Science Foundation (NSF) Grant GG-1024553. A. Dere received additional support from NSF GK-12: CarbonEARTH Grant EHR-0947962. The authors acknowledge K. Gaines, J. Wubbels, L. Smith and J. Kissel for green leaf and leaf litter collection and chemical analysis. We also acknowledge the Fall 2009 GEOSC 413 class at Penn State for their work collecting and analyzing samples at the SSHO as well as W. Castro, H. Gong, L. Liermann and J. Williams for analytical assistance. This work was facilitated by NSF Critical Zone Observatory program Grants to CJD (EAR 07-25019) and SLB (EAR 12-39285, EAR 13-31726). This research was conducted in Penn State's Stone Valley Forest, which is supported and managed by the Penn State's Forestland Management Office in the College of Agricultural Sciences.

References

- Alloway BJ (1995) Heavy metals in soils. Springer Science, Berlin
- Amundson R, Richter DD, Humphreys GS, Jobbagy EG, Gaillardet J (2007) Coupling between biota and earth materials in the Critical Zone. Elements 3:327–332. doi:10.2113/Gselements.3.5.327

- Anderson SP, Dietrich WE, Brimhall GH (2002) Weathering profiles, mass-balance analysis, and rates of solute loss: linkages between weathering and erosion in a small, steep catchment. Geol Soc Am Bull 114:1143–1158
- Barron AR, Wurzburger N, Bellenger JP, Wright SJ, Kraepiel AML, Hedin LO (2009) Molybdenum limitation of asymbiotic nitrogen fixation in tropical forest soils. Nat Geosci 2:42–45. doi:10.1038/ngeo366
- Brantley SL, Lebedeva M (2011) Learning to read the chemistry of regolith to understand the critical zone. Annu Rev Earth Planet Sci 39(39):387–416. doi:10.1146/Annurev-Earth-040809-152321
- Brantley SL, White AF (2009) Approaches to modeling weathered regolith. Thermodyn Kinet Water-Rock Interact 70:435–484. doi:10.2138/Rmg.2009.70.10
- Brimhall GH, Dietrich WE (1987) Constitutive mass balance relations between chemical-composition, volume, density, porosity, and strain in metasomatic hydrochemical systems-results on weathering and pedogenesis. Geochim Cosmochim Acta 51:567–587. doi:10.1016/0016-7037(87)90070-6
- Chappaz A, Lyons TW, Gordon GW, Anbar AD (2012) isotopic fingerprints of anthropogenic molybdenum in lake sediments. Environ Sci Technol 46:10934–10940. doi:10.1021/Es3019379
- Darnajoux R, Constantin J, Miadlikowska J, Lutzoni F, Bellenger JP (2014) Rapid report is vanadium a biometal for boreal cyanolichens? New Phytol 202:765–771. doi:10.1111/Nph.12777
- Dijkstra FA, Smits MM (2002) Tree species effects on calcium cycling: the role of calcium uptake in deep soils. Ecosystems 5:385–398. doi:10.1007/S10021-001-0082-4
- Dzombak DA, Morel FMM (1990) Surface complexation modelling: hydrous ferric oxide. Wiley-Interscience
- Eissenstat D et al (2013) Susquehanna Shale Hills Critical Zone Observatory Tree Survey (2008). Integrated Earth Data Applications (IEDA). doi:10.1594/IEDA/100268
- Fernando DR, Mizuno T, Woodrow IE, Baker AJM, Collins RN (2010) Characterization of foliar manganese (Mn) in Mn (hyper)accumulators using X-ray absorption spectroscopy. New Phytol 188:1014–1027. doi:10.1111/J.1469-8137. 2010.03431.X
- Gelinas Y, Lucotte M, Schmit JP (2000) History of the atmospheric deposition of major and trace elements in the industrialized St, Lawrence Valley, Quebec, Canada. Atmos Environ 34:1797–1810. doi:10.1016/S1352-2310(99)00336-2
- Gupta UC (1997) Molybdenum in agriculture. Cambridge University Press, Cambridge
- Hernandez L, Probst A, Probst JL, Ulrich E (2003) Heavy metal distribution in some French forest soils: evidence for atmospheric contamination. Sci Total Environ 312:195–219. doi:10.1016/S0048-9697(03)00223-7
- Herndon EM, Brantley SL (2011) Movement of manganese contamination through the critical zone. Appl Geochem 26:S40–S43. doi:10.1016/J.Apgeochem.03.024
- Herndon EM, Jin L, Brantley SL (2011) Soils reveal widespread manganese enrichment from industrial inputs. Environ Sci Technol 45:241–247. doi:10.1021/Es102001w
- Herndon EM, Martinez CE, and Brantley SL (2014) Spectroscopic (XANES/XRF) characterization of contaminant



- manganese cycling in a temperate watershed. Biogeochemistry 121:505-517
- Hodkinson BP et al (2014) Lichen-symbiotic cyanobacteria associated with Peltigera have an alternative vanadium-dependent nitrogen fixation system. Eur J Phycol 49:11–19. doi:10.1080/09670262.2013.873143
- Jean ME, Cassar N, Setzer C, Bellenger JP (2012) Short-term N2 fixation kinetics in a moss-associated cyanobacteria. Environ Sci Technol 46:8667–8671
- Jin L, Ravella R, Ketchum B, Bierman PR, Heaney P, White T, Brantley SL (2010) Mineral weathering and elemental transport during hillslope evolution at the Susquehanna/ Shale Hills Critical Zone Observatory. Geochim Cosmochim Acta 74:3669–3691. doi:10.1016/j.gca.2010.03.036
- Jobbagy EG, Jackson RB (2001) The distribution of soil nutrients with depth: global patterns and the imprint of plants. Biogeochemistry 53:51–77. doi:10.1023/A: 1010760720215
- Jobbagy EG, Jackson RB (2004) The uplift of soil nutrients by plants: biogeochemical consequences across scales. Ecology 85:2380–2389. doi:10.1890/03-0245
- Kaye MW, Smith L, Eissenstat D, Wubbles J, Adams T, Osborne J (2015) Susquehanna Shale Hills Critical Zone Observatory Tree Survey (2012 updates). EarthChem Library. doi:10.1594/IEDA/100516
- Kaye MW, Smith L, Eissenstat D (2016) Susquehanna Shale Hills Litter and Dendroband Data. EarthChem Library. doi:10.1594/IEDA/100517
- Kinkle BK, Angle JS, Keyser HH (1987) Long-term effects of metal-rich sewage-sludge application on soil populations of *Bradyrhizobium-japonicum*. Appl Environ Microbiol 53:315–319
- Kobler J, Fitz WJ, Dirnbock T, Mirtl M (2009) Soil type affects migration pattern of airborne Pb and Cd under a sprucebeech forest of the UN-ECE integrated monitoring site Zobelboden. Austria. Environ Pollut 158:849–854. doi:10. 1016/J.Envpol.09.026
- Kuntz BW, Rubin S, Berkowitz B, Singha K (2011) Quantifying solute transport at the shale hills critical zone observatory. Vadose Zone J 10:843–857. doi:10.2136/vzj2010.0130
- Lin H (2006) Temporal stability of soil moisture spatial pattern and subsurface preferential flow pathways in the shale hills catchment. Vadose Zone J 5:317–340. doi:10.2136/vzj2005.0058
- Lin HS, Kogelmann W, Walker C, Bruns MA (2006) Soil moisture patterns in a forested catchment: a hydropedological perspective. Geoderma 131:345–368. doi:10. 1016/j.geoderma.2005.03.013
- Lytle CM, Lytle FW, Smith BN (1996) Use of XAS to determine the chemical speciation of bioaccumulated manganese in *Potamogeton pectinatus*. J Environ Qual 25:311–316
- Ma L, Chabaux F, Pelt E, Blaes E, Jin L, Brantley S (2010) Regolith production rates calculated with uranium-series isotopes at Susquehanna/Shale Hills Critical Zone Observatory. Earth Planet Sci Lett 297:211–225. doi:10.1016/j. epsl.2010.06.022
- Ma L, Konter J, Herndon E, Jin L, Steinhoefel G, Sanchez D, Brantley SL (2015) Quantifying an early signature of the industrial revolution from lead concentrations and isotopes in soils of Pennsylvania, USA. Anthropocene. doi:10.1016/ j.ancene.2014.12.003

- Meij R, Winkel HT (2007) The emissions of heavy metals and persistent organic pollutants from modern coal-fired power stations. Atmos Environ 41:9262–9272. doi:10.1016/j. atmosenv.2007.04.042
- Naithani KJ, Baldwin DC, Gaines KP, Lin H, Eissenstat DM (2013) Spatial distribution of tree species governs the spatio-temporal interaction of leaf area index and soil moisture across a forested landscape. PLoS One 8:e58704
- Nriagu JO (1990) Global metal pollution-poisoning the biosphere. Environment 32:7–33
- Querol X et al (2007) Source origin of trace elements in PM from regional background, urban and industrial sites of Spain. Atmos Environ 41:7219–7231. doi:10.1016/J. Atmosenv.05.022
- Raven JA (1990) Predictions of Mn and Fe use efficiencies of phototrophic growth as a function of light availability for growth and of C assimilation pathway. New Phytol 116:1–18. doi:10.1111/J.1469-8137.1990.Tb00505.X
- Reimann C, Englmaier P, Flem B, Gough L, Lamothe P, Nordgulen O, Smith D (2008) Geochemical gradients in soil O-horizon samples from southern Norway: natural or anthropogenic? Appl Geochem 24:62–76. doi:10.1016/J. Apgeochem.11.021
- Roy M, McDonald LM (2013) Metal uptake in plants and health risk assessments in metal-contaminated smelter soils. Land Degrad Dev. doi:10.1002/ldr.2237
- Silvester WB (1989) Molybdenum limitation of asymbiotic nitrogen fixation in forests of Pacific Northwest America. Soil Biol Biochem 21:283–289
- Smith LA (2013) Aboveground carbon distribution across a temperate watershed. M.S. Thesis, The Pennsylvania State University, University Park
- Sucharova J et al (2012) Top-/bottom-soil ratios and enrichment factors: what do they really show? Appl Geochem 27:138–145. doi:10.1016/J.Apgeochem.09.025
- Sunda WG, Huntsman SA (1996) Antagonisms between cadmium and zinc toxicity and manganese limitation in a coastal diatom. Limnol Oceanogr 41:373–387
- Teutsch N, Erel Y, Halicz L, Chadwick OA (1999) The influence of rainfall on metal concentration and behavior in the soil. Geochim Cosmochim Acta 63:3499–3511. doi:10.1016/S0016-7037(99)00152-0
- Tyler G (2004) Vertical distribution of major, minor, and rare elements in a Haplic Podzol. Geoderma 119(277–290): 2003. doi:10.1016/J.Geoderma.08.005
- West N, Kirby E, Bierman P, Slingerland R, Ma L, Rood D, Brantley S (2013) Regolith production and transport at the Susquehanna Shale Hills Critical Zone Observatory, Part 2: insights from meteoric Be-10. J Geophys Res-Earth Surf 118:1877–1896. doi:10.1002/Jgrf.20121
- White AF, Schulz MS, Vivit DV, Bullen TD (2011) Fitzpatrick J (2012) The impact of biotic/abiotic interfaces in mineral nutrient cycling: a study of soils of the Santa Cruz chronosequence. Calif Geochim Cosmochim Acta 77:62–85. doi:10.1016/J.Gca.10.029
- Wichard T, Mishra B, Myneni SCB, Bellenger JP, Kraepiel AML (2009) Storage and bioavailability of molybdenum in soils increased by organic matter complexation. Nat Geosci 2:625–629. doi:10.1038/ngeo589
- Wubbels JK (2010) Tree species distribution in relation to stem hydraulic traits and soil moisture in a mixed hardwood



- forest in Central Pennsylvania. M.S. Thesis, The Pennsylvania State University, University Park
- Wurzburger N, Bellenger JP, Kraepiel AML, Hedin LO (2012) Molybdenum and phosphorus interact to constrain asymbiotic nitrogen fixation in tropical forests. PLoS One 7:e33710
- Xu Y, Morel FM (2013) Cadmium in marine phytoplankton. Met Ions Life Sci 11:509–528. doi:10.1007/978-94-007-5179-8_16
- Xu Y, Feng L, Jeffrey PD, Shi YG, Morel FMM (2008) Structure and metal exchange in the cadmium carbonic anhydrase of marine diatoms. Nature 452:56–61. doi:10.1038/Nature06636
- Yi SM et al (2006) Atmospheric dry deposition of trace elements measured around the urban and industrially impacted NY–NJ harbor. Atmos Environ 40:6626–6637. doi:10.1016/J. Atmosenv.05.062

